PAPER Nr.: 21

A CONSISTENT FINITE-VOLUME FORMULATION FOR THE SOLUTION OF THE NON-LINEAR POTENTIAL FLOW OVER A ROTOR BLADE

BY

L. GASPARINI AND L. VIGEVANO

DIPARTIMENTO DI INGEGNERIA AEROSPAZIALE, POLITECNICO DI MILANO
MILANO, ITALY

TWENTIETH EUROPEAN ROTORCRAFT FORUM
OCTOBER 4 - 7, 1994 AMSTERDAM

Printed by the Technical Highschool Haarlem

A Consistent Finite-Volume Formulation for the Solution of the Non-linear Potential Flow over a Rotor Blade

L. Gasparini, L. Vigevano
Dipartimento di Ingegneria Aerospaziale, Politecnico di Milano
via Golgi 40, 20133 Milano, Italy

Abstract

Finite-difference solutions of the unsteady full-potential equation (FPE) in strong conservation form are widely used to predict rotor aeroacoustic fields, because of the reasonably accurate physical description of the rotor aerodynamics and of the high computational efficiency. An important feature of finite-difference methods is consistency, which is defined as the capability of the numerical scheme to achieve perfect free-stream reproduction. Although specific consistency conditions have been developed in the past years for the steady FPE, their applications to three-dimensional problems still presents difficulties. Moreover, rotor flows are characterised by the non-uniform free-stream velocity seen by the rotating blades.

A fully consistent scheme for the unsteady three-dimensional FPE is presented, which has been developed using a finite-volume approach for the treatment of the geometric properties of the discretisation. Results are presented which numerically confirm that perfect free-stream reproduction is achieved when applied to grid undergoing arbitrary rigid-body motions. Also, results of computation for non-lifting rotor flows are shown and compared with that obtained using a finite-difference method which is not fully consistent in 3D.

1 Introduction

Finite-difference methods based on the unsteady, three-dimensional full-potential equation (FPE) in strong conservation form are a "state of the art" tool, currently employed to predict rotor aeroacoustic fields. The inviscid, irrotational approach has proven attractive because the FPE provides a reasonably accurate physical description of the rotor aerodynamics, for a wide range of flow conditions, while performing with greater computational efficiency than Euler or Navier-Stokes methods.

A very important feature of finite-difference methods, needed to achieve accurate solutions, is consistency. When using a boundary-conforming coordinate transformation and/or irregular grids, if the numerical scheme is not consistent the global conservation may be affected at discretised level and geometrical errors may arise, that reduce the accuracy of the scheme. Consistency is generally defined in an indirect way as the capability of the numerical scheme to achieve perfect free-stream reproduction, that is to reduce to zero the truncation errors associated with a free-stream distribution of the dependent variable.

Thomas and Lombard [1] first pointed out that, in order to preserve consistency, a geometrical conservation law (GCL) must be imposed, when solving the fluid dynamics equations using time dependent mappings. Hindman [2] showed that geometrically induced errors could occur when the consistency condition, obtained from the discrete form of the GCL, was violated. Specific consistency conditions for the steady, two-dimensional FPE were developed by Flores *et al.* [3]. Unlike the Euler and Navier-Stokes systems of equations, for which a single GCL has to be satisfied, the FPE requires three conditions: condition 1 on the metric differencing associated to the density calculation, and conditions 2 and 3 on the metric differencing associated to

the flux calculation. While the extension of the first two conditions to a three-dimensional flow is straightforward, the corresponding extension of the third condition is more difficult, requiring to simultaneously satisfy three geometric relations [3]. Moreover, no perfect free-stream reproduction conditions have been developed for the three-dimensional rotor problem.

As a result, many schemes that are fully consistent for the 2D FPE are not consistent when applied to the unsteady three-dimensional FPE. The problem has generally been solved using the 2D-consistent schemes with a correction technique that subtracts from the right hand side of the discretised equation the free-stream contribution [4]. The results obtained with this approach have been fairly satisfactory for engineering purposes. However, the free-stream subtraction technique can not be applied at the solid wall boundary, where loss of accuracy may arise.

In order to obtain a fully consistent 3D scheme for the steady FPE it is necessary not to use the same set of difference operators to satisfy all three consistency conditions, as suggested in [3]. In this way perfect free-stream reproduction is achieved for a steady potential flow and the subtraction technique need not to be applied. The latter approach has been employed in the development of the new version of the FPR code [5]. The improvement of the inviscid drag calculation with respect to the results of the inconsistent scheme of the original FPR code [6] is remarkable. Again, however, consistency is only approximate for the unsteady rotor flow calculations.

The present contribution deals with a fully consistent scheme for the unsteady three dimensional FPE, developed by separating the properties of the flow, from the geometry of the discretization. This approach calls for an integral formulation of the equation and can be viewed as a finite-volume scheme, although for potential flow, as pointed out by Vinokur [7], a clear distinction between finite-difference and finite-volume schemes can be made only about the way the cell geometry is handled.

The paper is subdivided in two main sections. The first section describes in some detail the new finite-volume method, while the second section presents some comparison of results, computed with the new approach and with a 2D-consistent method that represents the three-dimensional extension of the scheme described in [8].

2 Formulation

The complete formulation of the FPE model for the computation of unsteady flows around a single rotor blade will be presented. It is assumed that the blade is rigid and that its rigid body motion is known at each time, as is the velocity induced on the blade by the far wake.

All the velocities are normalised by the free-stream sound speed, a_∞, the lengths by the reference chord, l, the density by the free-stream value, ρ_∞, and the time by the value l/a_∞.

2.1 Integral form of the FPE

The FPE is derived from the Euler system of equations, under the assumption of isentropicity and irrotationality; both are considered acceptable for the transonic flows with moderate shock strength that develop around helicopter rotor blades. The former assumption may be relaxed adopting a non-isentropic, irrotational, full potential model, in which account is taken for the entropy production at the shocks [9]. In the following we will assume isentropic flow conditions.

With the aforementioned hypothesis the Euler system reduces to the mass-conservation equation, supplemented by the thermodynamic relations of a perfect gas and by Bernoulli theorem for the determination of the sound speed. If we consider the integral form of the mass-conservation equation, than the complete set of equations we are dealing with, written in a Cartesian frame of reference $\mathbf{x}', t$, is:

$$\frac{d}{dt}\int_V \rho\, dV + \oint_S \mathbf{n}' \cdot \mathbf{F}'\, dS = 0 \tag{1}$$

$$\mathbf{F}' = \rho(\mathbf{v}'_a - \mathbf{v}'_s) \tag{2}$$

$$\mathbf{v}'_a = \nabla'\phi \tag{3}$$

$$\rho = a^{\frac{2}{\gamma-1}} \tag{4}$$

$$a^2 = 1 - (\gamma - 1)\left(\phi_t + \frac{\mathbf{v}'^2_a}{2}\right) \tag{5}$$

where $\mathbf{v}'_a$ is the absolute fluid velocity, $\mathbf{v}'_s$ is the velocity of the surface element, so that $\mathbf{v}'_a - \mathbf{v}'_s$ is the relative velocity of the fluid with respect to the surface element, $\phi = \phi(\mathbf{x}', t)$ is the velocity potential, ρ is the density, a is the sound speed, and γ is the ratio of specific heats. The integrals are taken over an arbitrary region of volume V, delimited by the surface S, with outward normal versor $\mathbf{n}'$.

2.2 Integral form of the FPE in a body-fixed frame

It is convenient to introduce a non-inertial, body-fixed, Cartesian reference frame $\mathbf{x}, t$ given by:

$$\mathbf{x}' = \mathbf{x}'(\mathbf{x}, t) \tag{6}$$

Because of the assumed rigid body motion of the blade, the blade geometry will remain unchanged when viewed in this frame.

It is also convenient to consider the velocity vectors used in the previous equations, as well as all the other vector quantities, expressed in the body-fixed frame: in the notation we will write these vectors without the primes. For example, the velocity $\mathbf{v}_f$ of a point $\mathbf{x}$, fixed in the body frame, will be:

$$\mathbf{v}_f = \mathbf{v}_f(\mathbf{x}, t) = \mathbf{v}_0(t) + \boldsymbol{\Omega}(t) \times \mathbf{x} \tag{7}$$

where $\mathbf{v}_0$ is the velocity of the origin of the body-fixed frame relative to the inertial one and $\boldsymbol{\Omega}$ is its angular velocity, all expressed in the body frame.

To complete the change of perspective, the potential may be thought function of the time and of the coordinates relative to the body-fixed frame, as opposed to the inertial one, i.e. $\phi = \phi(\mathbf{x}, t)$. Then, writing the equations (1)–(5) in the non-inertial frame, only the Bernoulli relation undergoes a minor change, due to the presence of the time derivative of the velocity potential which becomes:

$$\frac{D\phi}{Dt} = \phi_t - \mathbf{v}_f(\mathbf{x}, t) \cdot \nabla\phi = \phi_t - \mathbf{v}_f \cdot \mathbf{v}_a \tag{8}$$

so that the integral form of the FPE may be written in the body-fixed reference frame as:

$$\frac{d}{dt}\int_V \rho\, dV + \oint_S \mathbf{n} \cdot \mathbf{F}\, dS = 0 \tag{9}$$

$$\mathbf{F} = \rho(\mathbf{v}_a - \mathbf{v}_s) \tag{10}$$

$$\mathbf{v}_a = \nabla\phi \tag{11}$$

$$\rho = a^{\frac{2}{\gamma-1}} \tag{12}$$

$$a^2 = 1-(\gamma-1)\left(\phi_t + \frac{\mathbf{v}_a{}^2 - 2\mathbf{v}_f\cdot\mathbf{v}_a}{2}\right) = 1-(\gamma-1)\left(\phi_t + \frac{\mathbf{v}_r{}^2 - \mathbf{v}_f{}^2}{2}\right) \tag{13}$$

where $\mathbf{v}_r = \mathbf{v}_a - \mathbf{v}_f$ is the fluid velocity relative to the body frame.

2.3 Finite-volume discretisation of the FPE

If we divide the flow region outside the body and inside an artificial far-field boundary surface into contiguous cells, we can apply eq. (9) to each of them, together with appropriate boundary conditions, to determine the values that the velocity potential function assumes at a point inside each cell.

To do this, it is necessary to define the geometry of the cells and the exact coordinates of the collocation points of the potential function. These are needed to compute the absolute fluid velocity from eq. (11). Mapping the Cartesian space around the body to a body-fitted coordinates system, through the transformation:

$$\xi = \xi(\mathbf{x},t) \quad \eta = \eta(\mathbf{x},t) \quad \zeta = \zeta(\mathbf{x},t) \tag{14}$$

the collocation points may be evenly spaced in the ξ,η,ζ computational volume, and derivatives with respect to the transformed coordinates are easily approximated using differencing schemes. Let $\mathbf{H}$ be the Jacobian matrix of transformation,

$$\mathbf{H} = \begin{bmatrix} \xi_x & \xi_y & \xi_z \\ \eta_x & \eta_y & \eta_z \\ \zeta_x & \zeta_y & \zeta_z \end{bmatrix} = \begin{bmatrix} x_\xi & x_\eta & x_\zeta \\ y_\xi & y_\eta & y_\zeta \\ z_\xi & z_\eta & z_\zeta \end{bmatrix}^{-1} \tag{15}$$

then eq. (11) becomes:

$$\mathbf{v}_a = \mathbf{H}^T\nabla\phi \tag{16}$$

where the gradient is now computed with respect to the coordinates ξ,η,ζ instead of x,y,z.

Suppose that a grid of collocation points for the potential function has been given, which is uniform in the computational space and conforms to the blade in the physical space: we will refer to this set of points as the *primary nodes* and to the hexahedral cells obtained by connecting the nodes with straight-line edges as the *primary cells*. The set of the centroids of the primary cells, defines an interlocking grid of *secondary nodes* which, in turn, subdivide the space into *secondary cells*, each having as centroid a primary node, i.e. a collocation points for the potential function. The integral form of the FPE will be applied to the secondary cells.

Note that if the blade is rigid, and if no grid adaptation is performed, then the coordinates transformation and the geometry of the cells are not time dependent, and the velocity of the surface elements, $\mathbf{v}_s$, is equal to the velocity of the body fixed frame, i.e. $\mathbf{v}_s = \mathbf{v}_f$.

When discretising eq. (9) over a finite number of given cells, the surface integral is replaced by the sum of integrals over the faces of the cell. These are approximated by the product of the flux, $\mathbf{F}$, at an average point on the face, by the surface area vector of the face; also, the volume integral is approximated by the product of the cell volume by the value of the density at an average point inside the cell:

$$\oint_S \mathbf{n} \cdot \mathbf{F}\, dS \approx \sum_{faces} \mathbf{s} \cdot \mathbf{F}(\mathbf{x}_S, t) \tag{17}$$

$$\int_V \rho\, dV \approx V \rho(\mathbf{x}_V, t) \tag{18}$$

where $\mathbf{s}$ is a vector normal to the face, directed outward, whose modulus is equal to the area of the face, V is the volume, constant, of the cell, and $\mathbf{x}_S, \mathbf{x}_V$ are respectively the centroids of the face and of the cell. These lead to the following finite-volume discretization of the integral form of the FPE:

$$\frac{d}{dt}\left[V \rho(\mathbf{x}_V, t)\right] + \sum_{faces} \mathbf{s} \cdot \mathbf{F}(\mathbf{x}_S, t) = 0 \tag{19}$$

If we want to guarantee that eq. (19) will be *exactly* satisfied by a uniform free-stream solution, thus avoiding the introduction of errors in the numerical scheme, some constraints must be imposed on the derivation of the geometric quantities used.

First, the sum of the surface area vectors of the cell faces must be equal to zero; this is the discrete counterpart of the integral statement which dictates the closure of the cell:

$$\oint_S \mathbf{n}\, dS = 0 \Leftrightarrow \sum_{faces} \mathbf{s} = 0 \tag{20}$$

Second, substituting eq. (10) and (7) into eq. (19), considering the density and the absolute fluid velocity to be equal to the constant free-stream values, and using relation (20), which is supposed to be satisfied, we find:

$$\sum_{faces} \mathbf{s} \cdot \mathbf{v}_f = 0 \Leftrightarrow \sum_{faces} \mathbf{x}_S \times \mathbf{s} = 0 \tag{21}$$

that is the discrete form of the integral condition (GCL) stating the conservation of the volume of the, supposed rigid, cell:

$$\oint_S \mathbf{n} \cdot \mathbf{v}_f\, dS = 0 \Leftrightarrow \oint_S \mathbf{x} \times \mathbf{n}\, dS = 0 \tag{22}$$

Finally, the sum of the cell volumes must be equal to the total volume of the flow region.

2.4 Time-integration of the FPE

The solution of the discretized finite-volume form of the FPE requires the calculation of the time derivative of the mass inside the cell. This derivative may be approximated with a first order backward difference:

$$\frac{d}{dt}\left[V \rho(\mathbf{x}_V, t)\right] \approx \frac{V}{\Delta t^n}\left[\rho(\mathbf{x}_V, t^{n+1}) - \rho(\mathbf{x}_V, t^n)\right] \tag{23}$$

with $\Delta t = t^{n+1} - t^n$, and where use has been made of the fact that the cell volume is constant. The indexes n and $n+1$ refer to two successive time instants.

Using this approximation, the integral form of the FPE, discretized in both space and time, results:

$$V(\rho^{n+1} - \rho^n) + \Delta t \sum \mathbf{s} \cdot \mathbf{F}^{n+1} = 0 \tag{24}$$

The value of the density as well as the values of the fluxes at time $n+1$ are complicate, non-linear, functions of the unknown potential, so that a Newton-like procedure seems well suited for the solution of the resulting system of non-linear equations [10]:

$$\mathbf{f}(\phi^{n+1}) = 0 \tag{25}$$

This procedure may be formulated as:

$$\mathbf{f}(\hat{\phi}) + \left(\frac{\partial \mathbf{f}}{\partial \phi}\right)_{\phi=\hat{\phi}} (\phi^{n+1} - \hat{\phi}) = 0 \tag{26}$$

where $\hat{\phi}$ represents the current estimate of the potential at time level $n+1$.

In order to start the Newton process, which is iterated until the correction $\Delta\phi = \phi^{n+1} - \hat{\phi}$ falls below a prescribed convergence value, a first guess of the solution at time level $n+1$ must be given.

An appropriate guess may be obtained [10] applying to eq. (25) a time-linearisation about level n, and solving for the potential correction $\Delta\phi = \phi^{n+1} - \phi^n$, that is:

$$\mathbf{f}(\phi^n) + \left(\frac{\partial \mathbf{f}}{\partial \phi}\right)_{\phi=\phi^n} (\phi^{n+1} - \phi^n) = 0 \tag{27}$$

This is equivalent to apply directly eq. (26) using as a first guess the value of the potential at the previous time level, ϕ^n, and a consistent extrapolation of the density value.

Both equation (26) and (27) result in a linear system, whose matrix is given by the Jacobian of eq. (25):

$$\left(\frac{\partial \mathbf{f}}{\partial \phi}\right) \Delta\phi = \mathbf{L}\Delta\phi = -\mathbf{f} \tag{28}$$

which can be solved introducing an approximate factorisation of the matrix $\mathbf{L}$:

$$\mathbf{L} \approx \mathbf{L}_\xi \mathbf{L}_\eta \mathbf{L}_\zeta \approx -\mathbf{f} \tag{29}$$

where each factor, containing only derivatives along one coordinate direction, is an easily invertible, narrow banded, matrix.

When solving eq. (24) for a Newton iteration step, using eq. (26), the values of the density and of the fluxes at time level $n+1$ are linearised as follows.

From equations (12), (13) and (16) one obtains:

$$\rho^{n+1} = \hat{\rho} + \left(\frac{\partial \rho}{\partial \phi}\right)_{\phi=\hat{\phi}} (\phi^{n+1} - \hat{\phi}) = \hat{\rho} - \frac{\hat{\rho}}{\hat{a}^2} \left(\frac{1}{\Delta t^n} + \hat{\mathbf{v}}_r \cdot \mathbf{H}^T \nabla\right) \Delta\hat{\phi} \tag{30}$$

The fluxes, given by eqn. (10) and (16), are approximately linearised as:

$$\mathbf{F}^{n+1} = \hat{\mathbf{F}} + \left(\frac{\partial \mathbf{F}}{\partial \phi}\right)_{\phi=\hat{\phi}} (\phi^{n+1} - \hat{\phi}) \approx \hat{\mathbf{F}} + \hat{\rho}\mathbf{H}^T \nabla \Delta\hat{\phi} \tag{31}$$

where the term

$$\hat{\mathbf{v}}_r \left(\frac{\partial \rho}{\partial \phi}\right)_{\phi=\hat{\phi}} \Delta\hat{\phi} = -\hat{\mathbf{v}}_r \frac{\hat{\rho}}{\hat{a}^2} \left(\frac{1}{\Delta t^n} + \hat{\mathbf{v}}_r \cdot \mathbf{H}^T \nabla\right) \Delta\hat{\phi} \tag{32}$$

has been neglected, in order to avoid the necessity of upwinding, thus obtaining easily invertible tri-diagonal factors.

A similar linearisation, with $1/\Delta t$ replaced by ∂_t, is employed when looking for a first guess solution using eq. (27).

2.5 Spatial discretisation

The correct way to compute the discretized fluxes through the cell faces, in order to satisfy the geometrical constraints expressed by conditions (20) and (21), will now be pointed out, following the suggestions of Vinokur [7].

Firstly, a clear distinction must be made, between the flow properties and the geometric and cinematic properties of the discretisation. In the case of the FPE the former ones are essentially represented by the absolute fluid velocity. The latter comprise the surface area vectors of the cell faces, the volumes of the cells and the part of the mass flux through the cell faces, induced *only* by the motion of the faces itself in the absolute reference frame.

As previously indicated, the components of the absolute fluid velocity are computed by taking the gradient of the potential function in the computational space and transforming it back to the physical space. The transformation matrix is the Jacobian of the coordinates transformation and is usually obtained by inverting the matrix of the derivatives of the cartesian coordinates with respect to the computational ones. It may be shown (see for example [11]) that, if the physical coordinates are numerically differenced with respect to the computational ones, in the *same way* as done for the potential, then the cartesian gradient of a potential function linearly dependent on the physical coordinates will be computed *exactly*, i.e. with no truncation errors. This means that a uniform velocity field will be exactly recovered.

Therefore, when computing the absolute fluid velocity from eq. (16), for the determination either of the density or of the fluxes, care must be taken that the same differencing scheme will be applied both to the potential and to the cartesian coordinates. This recommendation corresponds to the well-known consistency conditions 1 and 2, as expressed by Flores *et al.* [3].

In the present method, the density is computed only at the centroids of the primary grid cells, using a compact box differencing scheme. Simple averaging are then used to obtain the value of the density at the centroids of the faces of the secondary cells and at the centroids of the secondary cells, respectively for the calculation of the mass-fluxes and of the volume integrals. On the contrary, the absolute fluid velocity, also needed for the determination of the fluxes, is computed directly at the face centroids of the secondary cells.

The calculation of the geometric and cinematic properties of the discretisation scheme may be easily and rigorously done in the following manner.

Considering the secondary cells to be constructed as having straight-line edges, then, the surface area vector of a face, defined as:

$$\mathbf{s} = \int_S \mathbf{n}\, dS \tag{33}$$

is unique, depending only on the contour of the face and not on its particular "shape", in virtue of eq. (20). Therefore, a convenient shape may be chosen so as to simplify the computation of $\mathbf{s}$; for example, the face shape may be determined by the two plane triangle obtained by dividing the face with a diagonal, so that, referring to fig. 1, $\mathbf{s}$ will be given by:

$$\mathbf{s} = \mathbf{s}_A + \mathbf{s}_B = \frac{1}{2}\left(\mathbf{r}_{21} \times \mathbf{r}_{31} + \mathbf{r}_{31} \times \mathbf{r}_{41}\right) \tag{34}$$

where $\mathbf{r}_{ji}$ is the vector pointing from point $\mathbf{x}_i$ to point $\mathbf{x}_j$.

Similarly, the flux induced by the rigid motion of a face is unique, due to the fact that it must be equal to zero for a closed surface, as expressed by condition (21). It may be computed exactly, resorting to the same useful subdivision of the face into two plane triangle, as:

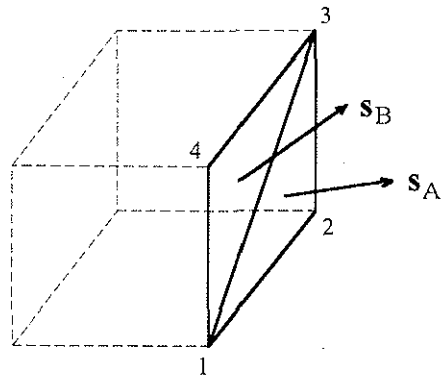

Figure 1: Computation of the surface area vector

$$\begin{aligned} \int_S \mathbf{n}\cdot\mathbf{v}_f\, dS &= \int_{S_A+S_B} \mathbf{n}\cdot(\mathbf{v}_0+\boldsymbol{\Omega}\times\mathbf{x})\, dS \\ &= (\mathbf{v}_0+\boldsymbol{\Omega}\times\mathbf{x}_{S_A})\cdot\mathbf{s}_A+(\mathbf{v}_0+\boldsymbol{\Omega}\times\mathbf{x}_{S_B})\cdot\mathbf{s}_B \end{aligned} \tag{35}$$

where $\mathbf{x}_{S_A}$ and $\mathbf{x}_{S_B}$ are the centers of the two triangular surfaces:

$$\begin{aligned} \mathbf{x}_{S_A} &= \frac{1}{3}(\mathbf{r}_1+\mathbf{r}_2+\mathbf{r}_3) \\ \mathbf{x}_{S_B} &= \frac{1}{3}(\mathbf{r}_1+\mathbf{r}_3+\mathbf{r}_4) \end{aligned} \tag{36}$$

While the surface area vectors and the fluxes induced across the faces by grid velocity are unique, given the straight-line edges definition of the cell, its volume is dependent on the particular shape of the faces. In order to obtain that the volumes of all the cells sum up to the volume of the space region considered, it is necessary to assume exactly the same face shape when computing the volumes of both cells sharing a face.

A convenient way to achieve this is to divide parallel faces of a cell with corresponding parallel diagonals, and assume the face shape to be the same union of two plane triangles used in the previous calculations. Then, the volume of the cell is obtained as the sum of the volumes of twelve tetrahedra, each defined by one of the twelve triangular sub-faces and by an auxiliary point inside the cell, chosen as common apex.

Recalling that the volume of a tetrahedron is one third of the scalar product of the surface area vector of the base, by a vector pointing from the apex to an arbitrary point on the base, e.g. referring to fig. 2:

$$V_{1234} = \frac{1}{3}\mathbf{s}_{123}\cdot\mathbf{r}_{14} \tag{37}$$

it may be argued that the volumes of the two tetrahedra corresponding to each cell face may be coupled, choosing the arbitrary point to lie on the diagonal dividing the face; that is:

$$V_{12345} = \frac{1}{3}(\mathbf{s}_{123}\cdot\mathbf{r}_{15}+\mathbf{s}_{134}\cdot\mathbf{r}_{15}) = \frac{1}{3}(\mathbf{s}_A+\mathbf{s}_B)\cdot\mathbf{r}_{15} = \frac{1}{3}\mathbf{s}\cdot\mathbf{r}_{15} \tag{38}$$

Therefore, the volume of the cell is equal to the sum of the volumes of six pyramids, each having as base an "equivalent plane face" containing a diagonal. Further, if the diagonals of all the cell faces, parallel two by two, are chosen so that they converge in two opposite vertices of the cell, then, taking one of these vertices as the common apex the six pyramids reduce to three. The volume of the cell may thus be efficiently computed, with reference to fig. 3 from:

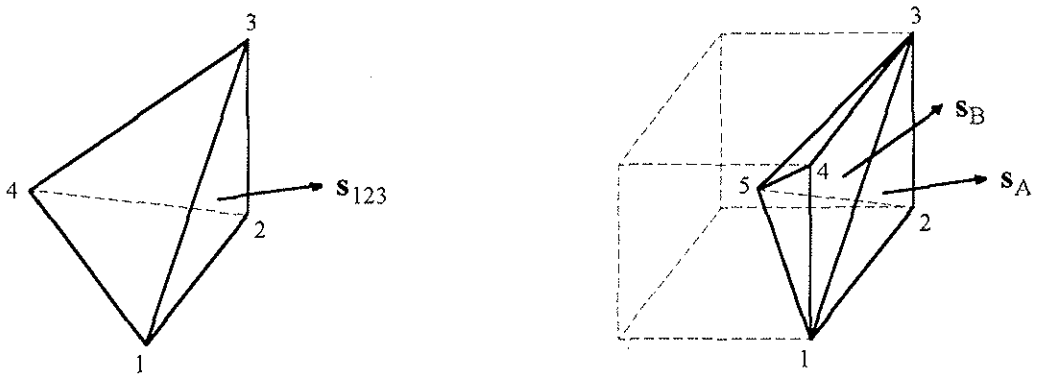

Figure 2: Volume of a tetrahedron and face contribution to the cell volume

$$V = \frac{1}{3}(\mathbf{s}_\xi + \mathbf{s}_\eta + \mathbf{s}_\zeta) \cdot \mathbf{r}_{21} \tag{39}$$

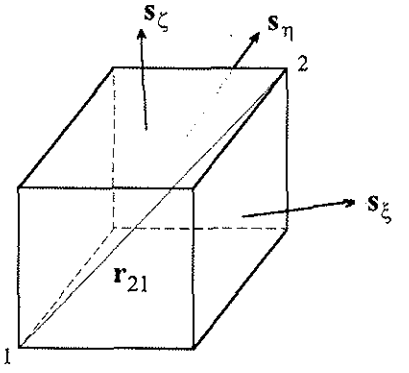

Figure 3: Computation of the cell volume

It should be remarked that four slightly different values of the cell volume derive from the four possible choices of consistent subdivision of the faces with converging diagonals: anyway, it is guaranteed that the total volume will sum up properly.

Having said that, the mass-flux across a cell face may be readily computed as:

$$\int_S \rho(\mathbf{v}_a - \mathbf{v}_f) \cdot \mathbf{n}\, dS \simeq \rho\left[(\mathbf{v}_a + \mathbf{v}_0) \cdot \mathbf{s} + \boldsymbol{\Omega} \times \mathbf{x}_{S_A} \cdot \mathbf{s}_A + \boldsymbol{\Omega} \times \mathbf{x}_{S_B} \cdot \mathbf{s}_B\right] \tag{40}$$

where the only approximation done, is to consider values of the density and of the absolute fluid velocity constant along the surface and equal to the values that they assume at the face centroid.

Due to the way all the quantities appearing in the previous relation are computed, in the case of a uniform free-stream flow, the mass-flux through the faces of a cell will sum exactly to zero, for every arbitrary rigid motion of the body-fixed frame. In fact, it may be shown that the correct computation of the surface area vectors corresponds to the application of the third consistency condition introduced by Flores *et al.* for the steady FPE, and really constitutes an easy and intuitive way to solve the three simultaneous relations that arise from this in the 3D case. Moreover, the careful evaluation of the fluxes induced by the grid velocity is equivalent to satisfying the GCL stated by Thomas and Lombard, and enforces the consistency of the scheme when dealing with arbitrary rigid grid motions.

2.6 Density biasing scheme

In the calculation of the fluxes, a biased value of the density is used to provide the necessary artificial viscosity needed to stabilise supersonic regions and capture shock waves properly.

The streamwise flux biasing technique, firstly introduced by Osher [12], is employed, with the biased value of density, $\tilde{\rho}$, given by:

$$\tilde{\rho} = \frac{1}{q}\left[\rho q - \left(\frac{U}{Q}\Delta\xi\frac{\partial}{\partial\xi} + \frac{V}{Q}\Delta\eta\frac{\partial}{\partial\eta} + \frac{W}{Q}\Delta\zeta\frac{\partial}{\partial\zeta}\right)(\rho q)^{-}\right] \tag{41}$$

where q is the modulus of the fluid velocity *relative* to the grid, U, V, W are the contravariant components of the relative velocity $\mathbf{V}$ in the transformed space ξ, η, ζ, obtained from

$$\mathbf{V} = \mathbf{H}\mathbf{v}_r \tag{42}$$

and Q is the modulus of $\mathbf{V}$. Further, the derivatives in eq. (41) are computed in the upstream direction with respect to the contravariant component of the relative velocity, and the quantity $(\rho q)^{-}$ is defined as:

$$\begin{array}{lcll} (\rho q)^{-} & = & \rho q - \rho^* q^* & q > q^* \\ (\rho q)^{-} & = & 0 & q \leq q^* \end{array} \tag{43}$$

Here the quantities $\rho^*, q^*, \rho^* q^*$ are the sonic reference values of the density, the relative velocity modulus and the relative density flux. The sonic value of the relative velocity may be easily determined from equation (13) by imposing $\mathbf{v}_r^2 = a^2 = (q^*)^2$, obtaining:

$$(q^*)^2 = \frac{1 - (\gamma - 1)(\phi_t - \mathbf{v}_f^2/2)}{(\gamma + 1)/2} \tag{44}$$

from which it follows:

$$\rho^* = (q^*)^{\frac{2}{\gamma - 1}} \tag{45}$$

2.7 Boundary and wake conditions

On the body, the usual inviscid flow conditions of no flux through the boundary is enforced by setting to zero the mass-flux across all the cell faces lying on the body contour. When solving for lifting rotor flows, this condition is modified to allow for a transpiration velocity equal to the one induced on the body by the far wake, becoming:

$$(\mathbf{v}_r + \mathbf{v}_i) \cdot \mathbf{n}_b = 0 \tag{46}$$

where $\mathbf{v}_i$ is the absolute wake induced velocity.

On the inboard hub plane, normal to the blade span-wise direction, the flow perturbation is considered to be two-dimensional, and the components of the absolute fluid velocity normal to the grid plane is required to be zero. Thus the mass-flux through the cell faces on the hub plane is given only by the flux induced by the grid velocity:

$$\mathbf{v}_a \cdot \mathbf{n}_h = 0 \leftrightarrow \mathbf{F} = -\rho \mathbf{v}_s \tag{47}$$

An implicit treatment of the boundary conditions at the body and at the hub plane is obtained by properly modifying the $\mathbf{L}_\xi, \mathbf{L}_\eta, \mathbf{L}_\zeta$ operators on the left hand side of equation (29).

On the wake cut behind the blade trailing edge the pressure and the normal component of the relative velocity are supposed to be continuous. These conditions result in a convection equation for the potential jump, $\Gamma = \phi_{up} - \phi_{low}$, across the cut:

$$\Gamma_t + \bar{U}\Gamma_\xi + \bar{V}\Gamma_\eta = 0 \tag{48}$$

where it has been supposed that the wake cut is represented in the computational space by a $\zeta = const$ plane, and where $\bar{U}, \bar{V}$ are the averaged contravariant ξ, η components of the relative fluid velocity on the upper and lower side of the cut.

At the outer boundary, non-reflecting far-field conditions are imposed, in the form of prescribed incoming Riemann invariants, based on the normal components of the absolute fluid velocity:

$$\mathbf{v}_a \cdot \mathbf{n} - \frac{2a}{\gamma - 1} = -\left(\frac{2a}{\gamma - 1}\right)_\infty \tag{49}$$

Equation (49) is linearised and approximately factored in as much the same way as the mass-conservation equation, and implicitly solved simultaneously with it.

3 Discussion of results

The consistency of the new finite volume method has been checked by computing the residuals, for a free-stream flow that is at rest in the absolute frame of reference. The residual values have been computed at each grid cell, except at those having one face right on the body boundary, which are inherently non free-stream consistent. Both the case of a simple translation of the body fixed-frame of reference, representative of a "wing-like" motion, and the case of a coupled translation and rotation of the body-frame, which represents the blade motion of a rotor in forward flight, have been investigated.

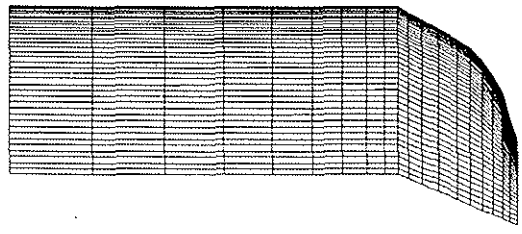

Figure 4: Blade planform and surface grid lines

The body is a typical helicopter rotor blade, with an "advanced geometry" parabolic tip planform, shown in fig. 4. The grid is a C-H sheared-parabolic grid, with $128 \times 32 \times 24$ cells respectively in the chord-wise, span-wise and normal directions, and 80×24 cells lying on the body boundary. It extends from .5 to 1.5 times the rotor radius, and approximately from four chords upstream to eight chords downstream of the blade leading edge.

In fig. 5 and 6 the number of grid points at which the residual is greater then a given value is plotted, for the new finite-volume scheme and for a finite-difference scheme that is only 2D-consistent [8]. The "rotor blade motion" refers to the blade in the azimuthal position $\psi = 90$ degrees of a rotor having an advancing ratio of $\mu = .45$.

It is evident that in the case of the wing motion, which is essentially 2D, both methods may be considered free-stream consistent from a practical point of view, giving residual values below 1E-13 at every node. On the contrary, in the case of the rotor blade motion, the finite-volume scheme preserves the consistency, while the finite-difference scheme suffers an abrupt increase in the values of the residuals. As a consequence, correction terms up to the order of 1E-2 should be

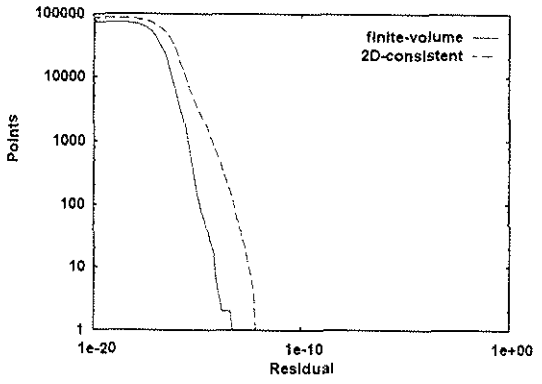

Figure 5: "Wing motion" residuals

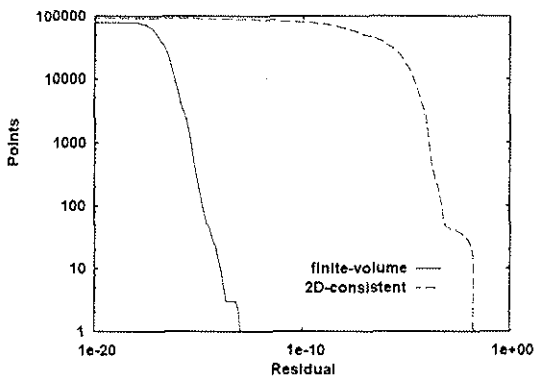

Figure 6: "Rotor blade motion" residuals

added to the residuals of the finite-difference scheme, to achieve perfect free-stream reproduction at the inner grid points.

Analogous results where obtained for different azimuthal position of the blade, and for different, rectangular or rectangular sweepback, blade tip planforms, confirming the capability of the finite-volume method to retain consistency for any rigid-body motion of the grid.

It should be noted that similar behaviours of the values of the residual have been obtained also for the blade of a hovering rotor, with large errors induced, in the finite-difference scheme, just by the simple rotation of the body-fixed frame.

Next, the effect of the different schemes — finite-volume and finite-difference with free-stream correction — on the accuracy of the computed results have been investigated. As reported by Bridgeman *et al.* [9], the greater impact is to be expected on the calculation of the wave drag.

Non-lifting hover computations, at increasing tip Mach number, were conducted with both codes, for the ONERA rectangular blade described in reference [13], using the same C-H grid previously described.

In fig. 7 it is plotted the computed torque coefficient, $C_Q = Q/\left(\rho \Pi R^3 (\Omega R)^2\right)$, relative to the outboard half span of the blade, versus the tip Mach number.

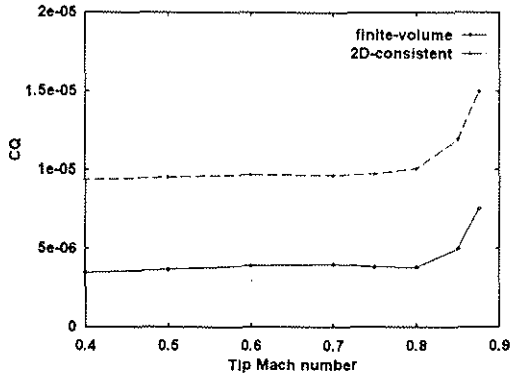

Figure 7: Torque coef. versus tip Mach number

Because the flow is supposed to be inviscid, the torque coefficient should be equal to zero when the flow remains entirely subsonic, that is until the tip Mach number reaches a value slightly above 0.8. The small positive torque computed at this lower tip speeds, must therefore be regarded as an error, due to an incorrectly evaluated small profile drag, and constitutes a tare which should be subtracted from the computed torque coefficient. This tare is remarkably constant, and may be quantified, considering the blade planform, in an average profile drag of $C_D = .0015$ and $C_D = .0006$ respectively for the finite-difference and for the finite-volume

solutions. The reduction of the tare drag to the very low value of approximately six counts confirms that a significant improvement in the accuracy of the estimated wave drag may be expected using a fully consistent discretisation of the FPE.

The influence of the numerical scheme on the computed pressure coefficient distribution on the blade is, however, very small. In fig. 8–10 the computed results are compared with the experimental values obtained at ONERA [13] for a rectangular blade with a 30 degrees sweepback tip in non-lifting, high-speed forward flight condition.

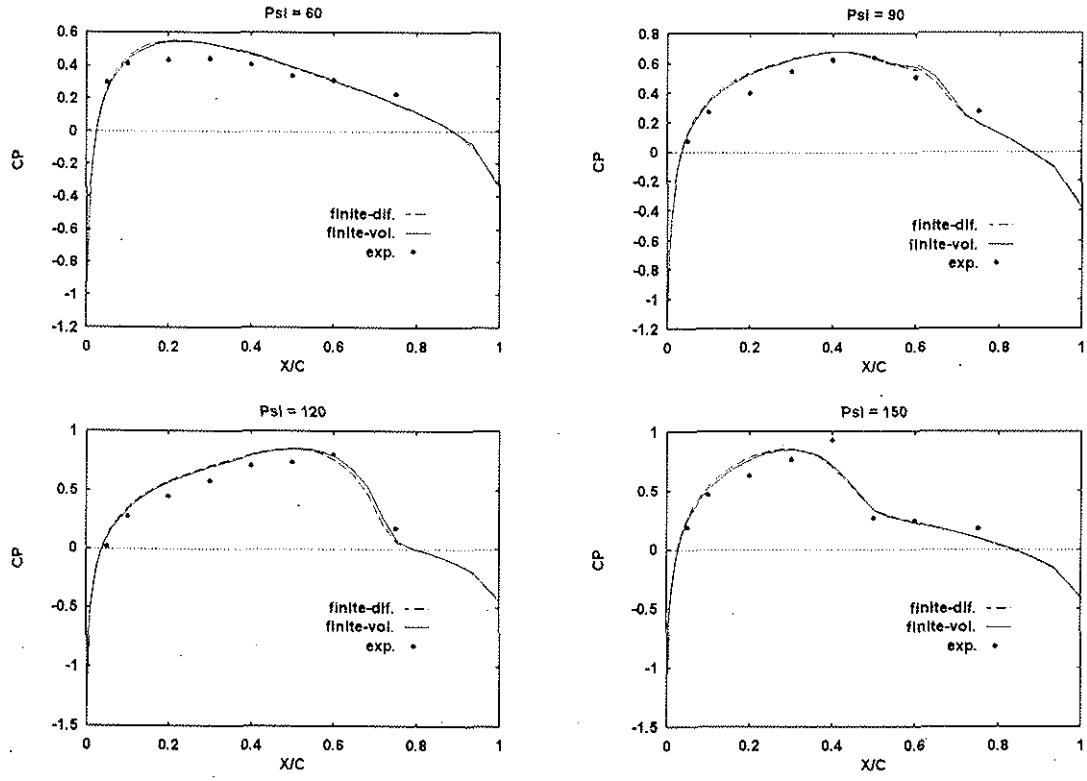

Figure 8: ONERA F30 blade, $M_{tip} = .625, \mu = .50, Z/R = .85$

The pressure distributions are displayed at the three span-wise station situated at the 85, 90 and 95 percent of the rotor radius, and, while generally in good agreement with the experimental data, show no clear evidence of improvement when going from the finite-difference to the finite-volume solution.

Both computations where performed with a time step that corresponds to a rotation of the blade of one third of degree, and just one Newton iteration was used to achieve time accuracy. It should be recalled that the finite-volume scheme requires the calculation of the metrics of the coordinates transformation and of the area vectors and volumes of the cells, as opposed to the finite-difference scheme for which only the metrics are needed. This results in a slightly degradation of the computational performance, of about 10 percent, due to the fact that, in order to reduce the memory requirements, all the geometric quantities are recomputed when needed instead of being stored. It should be noted that no attempt has been made to optimise neither the finite-difference nor the finite-volume code, and that the comparison has been made running both code on a scalar machine.

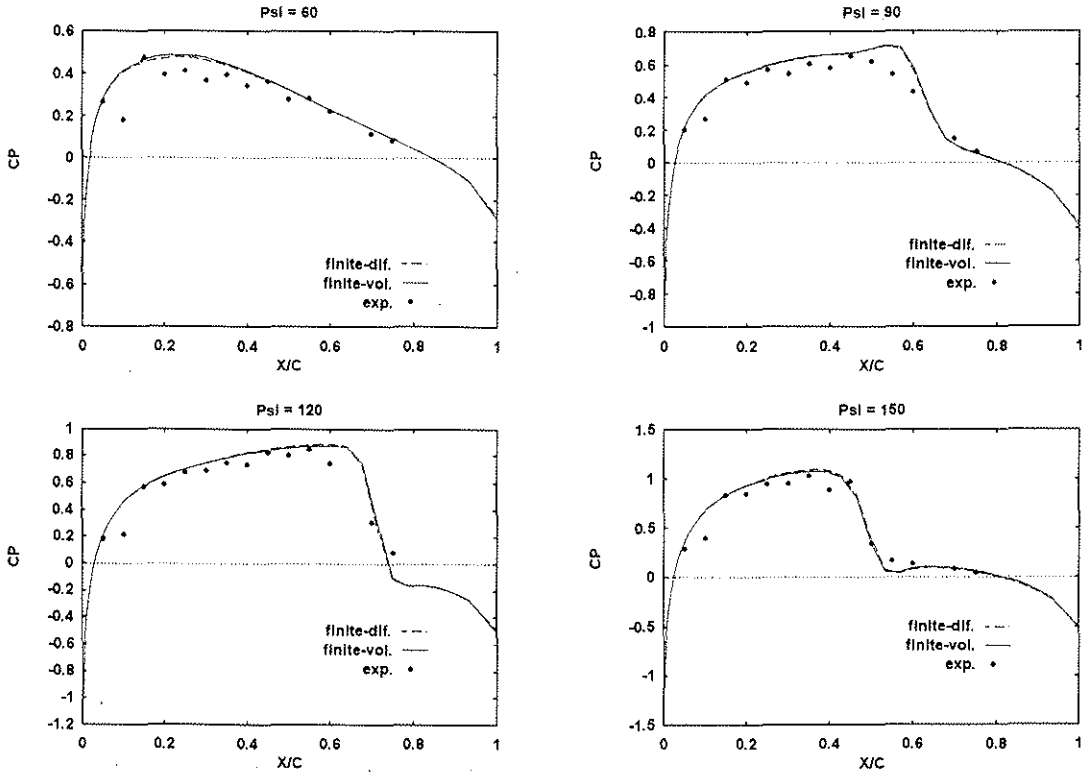

Figure 9: ONERA F30 blade, $M_{tip} = .625, \mu = .50, Z/R = .90$

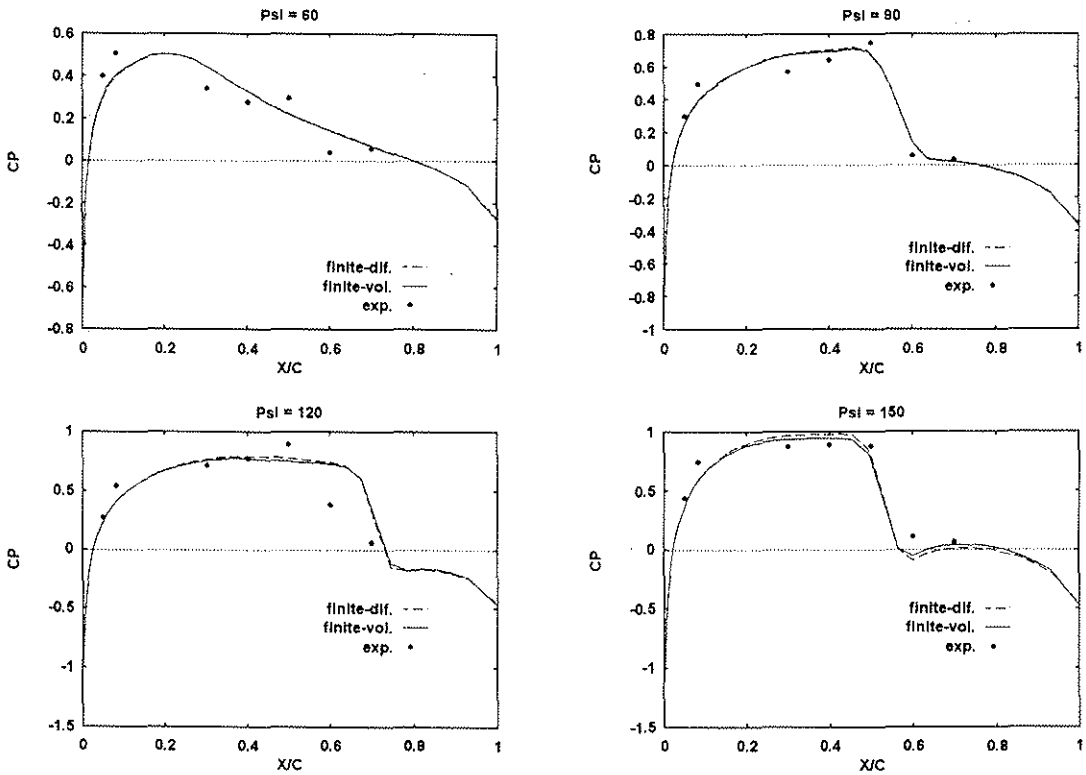

Figure 10: ONERA F30 blade, $M_{tip} = .625, \mu = .50, Z/R = .95$

4 Conclusion

A fully consistent finite-volume scheme for the unsteady full potential equation has been presented, which has the capability to reproduce exactly an unperturbed free-stream flow, when the computational grid undergoes an arbitrary rigid-body motion. This property has been confirmed by numerical experiments, showing that residual values lower then 1E-13 are obtained, even for a rotating, highly distorted, grid resulting from a complex geometry of the blade tip.

Calculations conducted for a non-lifting blade in hover, at different tip Mach numbers, indicate that an improvement in the evaluation of the profile wave drag is obtained, with respect to a formulation that is only partially consistent. This is achieved with a small increase in the computational costs. Instead, no significant changes are noticed in the predicted overall distribution of the pressure coefficient, over the blade of a non-lifting rotor in forward flight.

Although currently developed for application to grid experiencing rigid-body motions, the present formulation may be readily extended to deforming grids, giving the possibility to accurately compute unsteady flows about an elastic rotor blade using solution-adaptive grid.

References

[1] P.D. Thomas, and C.K. Lombard, Geometric Conservation Law and Its Application to Flow Computations on Moving Grids, *AIAA J.*, **17**, pp.1030-1037, 1979.

[2] R.G. Hindman, Generalized Coordinate Forms of Governing Fluid Equations and Associated Geometrically Induced Errors, *AIAA J.*, **20**, pp. 1359-1367, 1982.

[3] J. Flores, T.L. Holst, D. Kwak, and D.M. Batiste, A New Consistent Spatial Differencing Scheme for the Transonic Full-Potential Equation, *AIAA J.*, **22**, pp. 1027-1034, 1984.

[4] M. Costes, and H.E. Jones, Computation of Transonic Potential Flow on Helicopter Rotor Blades, paper presented at the 13th European Rotorcraft Forum, Arles, France, 1987.

[5] J.O. Bridgeman, R.C. Strawn, F.X. Caradonna, and C.S. Chen, Advanced Rotor Computations with a Corrected Potential Method, paper presented at the 45th Annual AHS Forum, Boston, MA., USA, 1989.

[6] R.C. Strawn, and F.X. Caradonna, Conservative Full-Potential Model for Usteady Transonic Rotor Flows, *AIAA J.*, **25**, pp. 193-198, 1987.

[7] M. Vinokur, An Analysis of Finite-Difference and Finite-Volume Formulations of Conservation Laws, *J. Comp. Phys.*, **81**, pp. 1-52., 1989.

[8] D. Ambrosi, L. Gasparini, and L. Vigevano, Full Potential and Euler Solutions for Transonic Unsteady Flow, paper presented at XXII Congresso Nazionale AIDAA, Como, Italy, 1993.

[9] J.O. Bridgeman, R.C. Strawn, and F.X. Caradonna, An Entropy and Viscosity Corrected Potential Method for Rotor Performance Prediction, paper presented at the 44th Annual AHS Forum, Boston, MA., USA, 1988.

[10] V. Shankar, H. Ide, J. Gorski, and S. Osher, A Fast, Time-Accurate, Unsteady Full Potential Scheme, *AIAA J.*, **25**, pp. 230-238, 1987.

[11] J.F. Thompson, Z.U.A. Warsi, and C.W. Mastin, Numerical Grid Generation, Foundations and Applications, North-Holland editions, 1985.

[12] S. Osher, M. Hafez, and W. Withlow Jr., Entropy Condition Satisfying Approximations for the Full Potential Equation of Transonic Flow, *Math. Comp.*, 44, pp. 1-29, 1985.

[13] J.J. Philippe, and J.J. Chattot, Experimental and Theoretical Studies on Helicopter Blade Tip at ONERA, paper presented at the 6th European Rotorcraft and Powered Lift Aircraft Forum, 1980.